2023-01-0494

Systematic Development Approach for a Hybrid Electric Powertrain Using Fuel-Cell-in-the-Loop Test Methodology[1]

Christoph Steindl and Peter Hofmann
TU Wien

Abstract

A promising approach for defossilization in the transport sector is using the polymer electrolyte membrane fuel cell (PEMFC) as an energy converter for propulsion in combination with green hydrogen. Furthermore, hybridization can bring an additional gain in efficiency. In a hybrid electric vehicle (HEV) powertrain, including FCHEV, at least two power sources (e.g., an FC system (FCS) with a hydrogen storage system and a high-voltage battery (HVB)) provide the required propulsion power. Thus, the powertrain topology and the energy management strategy (EMS) of an FCHEV are more complex than those of a conventional powertrain. To ensure a cost- and time-efficient development process, the FCHEV powertrain concept and its functions must be verified and evaluated early. To this end, this study presents the design and setup of an FC-in-the-Loop (FCiL) test platform as a tool for the systematic development of an FCHEV powertrain under realistic operating conditions. Hence, a medium size FCHEV is modeled with quasistatic sub-models of the powertrain components. The full-vehicle model is validated against measurement data of a commercially available FCHEV on a 4-wheel chassis dynamometer in a driving cycle. Based on the FCiL test methodology, the sizing of the FCS and HVB is demonstrated. It is found that for a low-load driving cycle such as the WLTC, a 110 kW FCS and a 1.6 kWh HVB can achieve a good result regarding low hydrogen consumption. Furthermore, two different EMS schemes, the power follower strategy (PFS) and the equivalent consumption minimization strategy (ECMS), are implemented and evaluated. With the ECMS, hydrogen consumption can be reduced by 1.6 % compared to the PFS. Moreover, the trade-off behavior between minimum hydrogen consumption and reduced dynamics of the FCS is investigated. Reducing the dynamic operation of the FCS by one-third results in an additional hydrogen consumption of only about 0.8 %.

Introduction

To achieve the defossilization of the transport sector, alternative propulsion concepts have increasingly become the focus of attention in research activities in the automotive industry in recent years. Next to the Battery Electric Vehicle (BEV), the Fuel Cell Electric Vehicle (FCEV), combined with green hydrogen, can play an essential role in the transformation process from fossil driven to local zero-emission propulsion systems. The advantages of the PEMFC, which make it attractive for use as an energy converter for propulsion in vehicles, are high efficiency, simplicity, no toxic emissions, high power density, and low operating temperature [1, 2]. Despite these positive aspects of the PEMFC technology, some challenges exist, especially durability and cost [3, 4, 5]. These issues must be overcome before the PEMFC can make a commercial breakthrough and achieve a significant market share as an energy converter for vehicle propulsion. The durability of the PEMFC is mainly affected by the transient operation of the PEMFC due to dynamic load requests in vehicles [6,7]. During frequent load changes, stress factors occur for the PEMFC, such as hydrogen and oxygen undersupply. These lead to a degradation of the corresponding electrodes and subsequently to a degradation of the performance of the PEMFC [8]. Thus, it is crucial to test the fuel cell system (FCS) and verify its functionality during the development process under transient operating conditions such as those in an automotive application.

Hybridization of the powertrain can contribute to overcoming the lifetime issue of the PEMFC and thus improving its reliability. Likewise, it enables a reduction of the energy demand for propulsion [9, 10]. In particular, a combination of an FCS, a hydrogen storage system (HSS), and a second power source, like a traction battery, in a fuel cell hybrid electric vehicle (FCHEV) can reduce hydrogen consumption. Actual available large-volume production FCEVs (e.g., Toyota Mirai 2nd Gen., Hyundai Nexo) are designed as an FCHEV. They use a traction battery as a secondary power source [11, 12]. In an FCHEV, both energy sources can independently provide the energy necessary for propulsion. In this context, a reliable energy management strategy (EMS) is needed. The main task of the EMS is to control the power split between the FC system and the traction battery considering the actual power demand of the driver [13]. Overall, an FCHEV results in a more complex powertrain topology and energy management strategy than a conventional powertrain. Thus, the development of an FCHEV is more challenging. For example, more effort must be made to verify and evaluate the EMS and its various functions. This makes it necessary to do the testing for verification and validation of the EMS at an early stage of the development process to be efficient in terms of cost and time [14,

[1] This is the peer-reviewed version of the following article: Steindl, C. and Hofmann, P., "Systematic Development Approach for a Hybrid Electric Powertrain Using Fuel-Cell-in-the-Loop Test Methodology," SAE Technical Paper 2023-01-0494, 2023, which has been published in final form at https://doi.org/10.4271/2023-01-0494.

15]. Therefore, the Hardware-in-the-Loop (HiL) test methodology in the automotive industry is well-established and a common development approach [16, 17]. A HiL platform consists of a physical and a virtual subsystem. The so-called hardware under test (HUT) represents the physical part. The real-time simulation of the remaining system depicts the virtual subsystem. Both subsystems are connected via a physical interface and constantly exchange information [18, 19, 20]. Based on this bidirectional information flow between the subsystems, effects due to the interaction are considered, and thus an investigation of the HUT under realistic conditions is enabled. Furthermore, parameters in the virtual environment can be easily adapted and optimized, as expected from offline simulation [21, 22].
Fuel-Cell-in-the-Loop (FCiL) is a specific form of HiL, where the FC system is the investigated hardware embedded in the real-time simulation environment. In the existing literature, a limited number of studies utilize the FCiL test methodology for development in automotive applications. R.M. Moore et al. [23, 24] introduced the FCiL test methodology for automotive applications. They presented it for use in designing and evaluating FCs and FC systems. In Ref. [25], with the help of the FCiL test methodology, the transient power response of the FC system is assessed, and the control algorithm of the boost converter used by the FCS is validated. Some FCiL platforms have been used to design and evaluate different EMSs [26, 27, 28, 29, 30]. The studies mentioned before utilize a reduced-scale approach for their FCiL platforms due to lower costs and less complex test stands than a full-size HiL platform. Here an FCS with a lower maximum output power than the actual system is used. In the existing literature, typically, lab-scale FCS are investigated with a maximum power range from 500 W to 1.2 kW. These lead to scale factors for the output power of the FC system from 8 to 267, depending on the vehicle application.
Nevertheless, based on literature analysis, two particular lacks are identified regarding the development process of FCHEV powertrains.

- There is a particular shortcoming regarding the interrelated powertrain design and validation process of an FCHEV powertrain. Validation of the system, and thus information on whether or not the system meets the requirements for the intended use, is an essential part of the development process. Furthermore, simultaneous development is crucial due to the coupling of powertrain design and the EMS of an FCHEV [31]. There is a gap in the existing literature regarding the two aspects mentioned before. This is because, on the one hand, in the studies discussed earlier, the design of the powertrain components was considered independently from the EMS in the design and evaluation using the FCiL test methodology. On the other hand, only a simultaneous development of the powertrain components and the EMS of FCHEV is carried out based on purely simulative studies without experimental evaluation, as in [32, 33, 34].

- Another gap exists in evaluating FCHEV powertrains and the respective EMS under realistic conditions. In available studies, the reduced-scale approach for FCiL platforms is chosen for the reasons mentioned earlier, such as less complexity and lower costs. The validity range of investigations with small scale factors is limited due to the associated assumptions.

This contribution aims to establish a systematic development approach of powertrain concepts and EMSs of an FCHEV using FCiL test methodology. In addition, the current work shall provide a step toward an evaluation under more realistic conditions of designed FCHEV powertrains and respective EMSs by introducing an FCiL platform with a medium size FC system.
This study is structured as follows. The first section deals with the principles of the systematic development approach. This section also contains the modeling of the full-vehicle model of an FCHEV and its validation against measurement data of a commercially available FCHEV on a 4-wheel chassis dynamometer in a driving cycle, the development of EMSs as well as the design and setup of the FCiL test methodology. The second section outlines the results of powertrain component sizing and assessment of different EMSs obtained with the FCiL platform. The final section summarizes the work and highlights the most significant findings.

Methodology

This section first gives an overview of the principle workflow of the holistic development approach for FCHEV powertrains. Then the numerical and experimental methods used for the investigations are outlined.

Development Approach

A holistic approach is chosen for designing and evaluating powertrain concepts and EMSs of an FCHEV. The workflow of this systematic methodology can be seen in Figure 1. Initially, a pure simulative design of powertrain concepts and EMSs is conducted. Subsequently, promising variants are evaluated at the test stand in the FCiL operation. As part of a feedback loop, the findings of this evaluation can be fed into future developments.

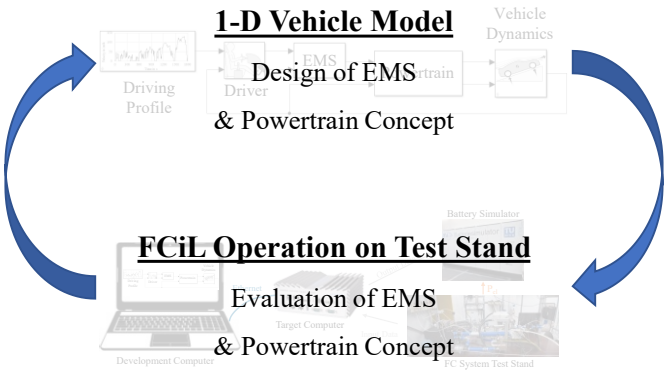

Figure 1 Workflow for design and evaluation of powertrain concepts and EMSs of an FCHEV

Studied FCHEV Powertrain

The investigations within this work are carried out with a generic FCHEV. The main parameters of the powertrain components are based on 2016 Toyota Mirai data, except for the FCS. The data basis for the FCS is a scaled-up version, which is implemented on the test stand and described later in this article. The main reason for selecting the 2016 Toyota Mirai is that measurement data on a 4-wheel chassis dynamometer in a driving cycle is available in Ref. [35] to validate the vehicle's longitudinal dynamics. However, the full-vehicle model is set up so that it can be easily re-parameterized and validated when other data is available. The principal layout of the modeled powertrain topology is shown in Figure 2.

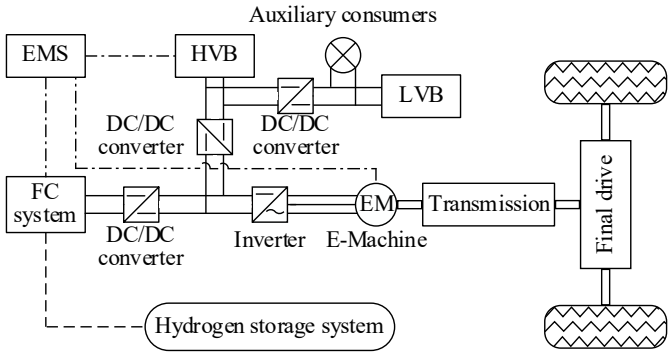

Figure 2 Powertrain architecture of the modeled FCHEV

The hydrogen storage system feeds the FCS with hydrogen. The FCS is connected to the high-voltage (HV) DC bus with a unidirectional DC/DC converter. In contrast, the HV battery (HVB), also known as the traction battery, is coupled by a bidirectional DC/DC converter with the HV DC bus. This enables the charging and discharging of the HVB. The low-voltage (LV) DC bus consists of auxiliary consumers (e.g., lighting system, power steering, etc.), and the LV battery (LVB) is linked via a DC/DC converter to the HVB. Further down the line, the HV DC bus provides the required electrical power through an inverter to the E-Machine (EM). The mechanical propulsion power of the EM is then supplied to the wheels via the drive shaft of the EM, a single-speed transmission, and a final drive.

Modeling

The model of an FCHEV is set up in the simulation environment MATLAB/Simulink. The modeling focuses on the FC hybrid powertrain's longitudinal dynamics and energy management. Thus, a forward modeling approach is chosen to simulate the longitudinal vehicle dynamics of the FCHEV. In this model approach, a time-dependent velocity profile is specified, and a driver model is used to calculate the necessary accelerator or brake pedal position based on the control difference between the actual speed of the vehicle and the reference speed of the driving profile. In the EMS, the driver commands are converted into a power demand for acceleration or deceleration. Accordingly, if an acceleration is requested decision about power allocation between the FCS and the HVB is made. In this context, the EMS makes a power request to the FCS and the HVB. These supply the E-Machine with the necessary power for propulsion, considering their respective limits. This information and power flow direction correspond to the action direction in real vehicle applications. Therefore, this modeling approach enables a good representation of reality. Figure 3 shows an overview of the full-vehicle model. It mainly consists of the driving profile, driver, energy management strategy, powertrain, and vehicle dynamics models. The following is a brief discussion of the sub-models used. The powertrain components are modeled based on the approaches presented in [36].

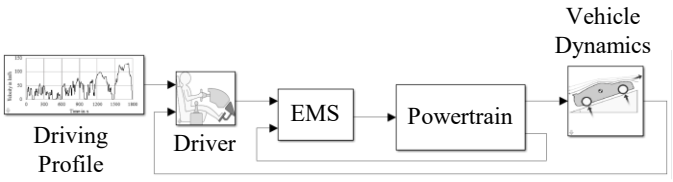

Figure 3 Full-vehicle model of the investigated FCHEV

Driving Profile

The evaluation of the hydrogen consumption for different powertrain concepts and EMSs is conducted based on the worldwide harmonized light vehicles test cycle (WLTC) class 3b driving profile. For validation purposes of the vehicle dynamics model and part of the powertrain model, the ADAC Eco-Test cycle is used. Figure 4 depicts the velocity profiles as a function of time for the investigated driving cycles.

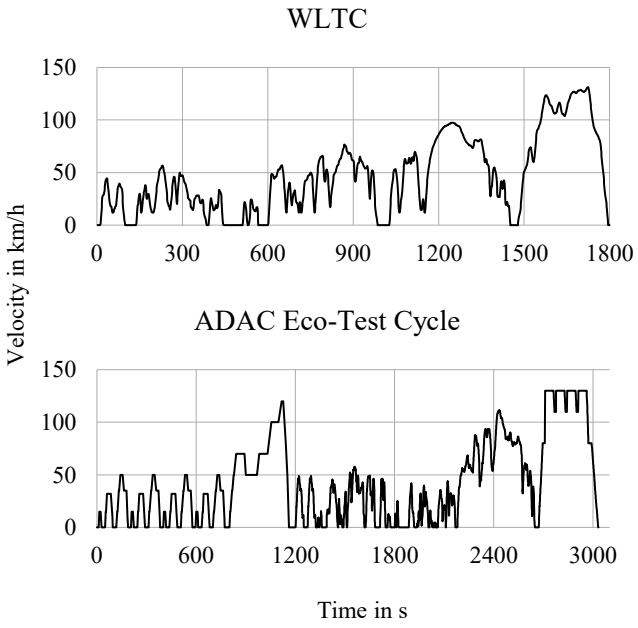

Figure 4 Velocity profiles of the investigated driving cycles

Driver

The inputs of the driver model are the reference vehicle velocity coming from the driving profile and the actual vehicle velocity, which is calculated in the vehicle dynamics model. The driver model determines the difference between the before mentioned velocities. Subsequently, driver commands are generated to minimize the control difference. These commands are then sent to the EMS for further processing. In this work, a proportional-integral (PI) controller is utilized to mimic the behavior of a real driver.

Energy Management Strategy

The main task of the energy management strategy is to allocate the power optimally between the different sources of the hybrid electric powertrain, always following the driver's power demand. In an FCHEV, the EMS regulates the interaction between the fuel cell system and the secondary energy source, which is, in this study, a traction battery. Thus, the EMS substantially influences the multiple sources operating range and operating conditions. This implies a significant effect on hydrogen consumption and powertrain component lifetime and enables the definition of specific objectives (e.g., hydrogen consumption minimization, component degradation reduction, etc.), which EMS shall consider.
There exists a variety of approaches for EMSs. As described in [37, 38, 39, 40], they can be classified into two main categories, rule-based and optimization-based.
The rule-based approaches rely on pre-defined rules and regularities.

Hence, they profit from their simplicity with the main disadvantage of obtaining not optimal power split solutions. In contrast, optimization-based EMSs are characterized by using an algorithm to minimize a cost function considering specific constraints (e.g., battery state of charge, power limits). Inherently they can obtain optimal solutions regarding power allocation, but with the decisive drawback of requiring more computational effort compared to the rule-based EMSs [41, 42].

This study focuses on a systematic approach to EMS development for FCHEV. For this purpose, a base EMS is designed and evaluated regarding the trade-off between minimum hydrogen consumption and reduced dynamic operation of the FCS. The latter can be seen as a measure on the system level to prolong FC lifetime. In addition, a second EMS is developed and used to compare representatives of the different approaches for EMS regarding solution quality. Therefore, already existing schemes of EMS are used as a basis for further development and optimization.

The base EMS in this article is the power follower strategy (PFS), also called the load follower strategy, a rule-based EMS. It is a well-known scheme used by several authors [43, 44, 45] as EMS in an FCHEV. The basic idea behind this EMS is that the FCS serves as the primary power source and follows the transient load requirements. A power range ($P_{FCS,\,min}$, $P_{FCS,\,max}$) is defined to operate the FCS with the highest possible efficiency. The HVB compensates for the differences between the FC system's output power and the driver's demanded power. The operating state of the FCS depends on the current state of charge (SoC) of the HVB and its power limits, as well as on the power limits of the FCS. Figure 5 shows the main rules for turning the FCS on and off.

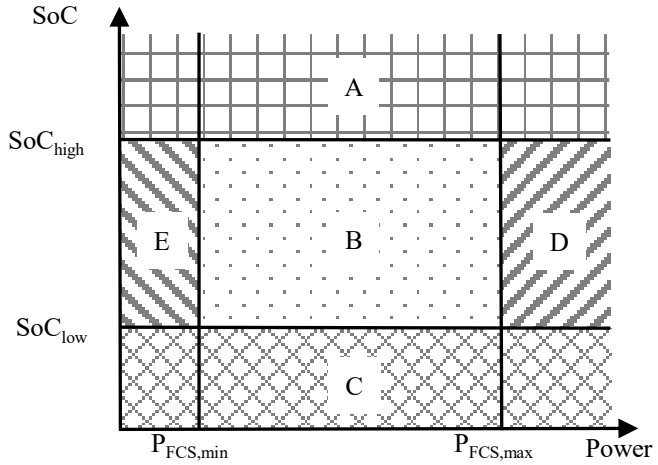

Figure 5 Main rules of the power follower strategy

When the SoC of the HVB falls below the lower limit SoC_{low}, the FCS is activated, regardless of the required power (zone C). If an operating point in zone B is reached, the FCS is activated and follows the load demand. Furthermore, the FCS remains active if the SoC is between the limit values SoC_{low} and SoC_{high}, and a power is requested that exceeds the maximum allowed output power of the FCS $P_{FCS,\,max}$. In this case, the FCS is operated at its maximum power $P_{FCS,\,max}$ (zone D). The difference between the maximum power of the FCS and the power demand is provided by the HVB, considering its power limits. The FCS is switched off when the actual SoC of the HVB exceeds the SoC_{high} limit (zone A). Furthermore, the FCS is switched off when the value of SoC is between the limit values SoC_{low} and SoC_{high}, but the requested power is lower than the minimum allowed power of the FCS $P_{FCS,\,min}$ (zone E). In addition, the FCS is operated when the power demand exceeds the maximum permissible power of the HVB.

An optimization-based approach is chosen as the second EMS, the so-called equivalent consumption minimization strategy (ECMS). For the first time, the ECMS for application in an FCHEV was introduced by Paganelli et al. [46]. Since then, several authors [47, 48, 49] have widely used and further developed it. The ECMS is based on the two fundamental thoughts that in an HEV, all the energy used for propulsion ultimately comes from the chemical energy carrier, such as hydrogen, and the battery is only used as an intermediate energy buffer. Any electrical power drawn from the battery during a discharge phase must later be fed back to the battery using hydrogen in the FCS or through recuperation. The operating principle of the ECMS is given in Figure 6.

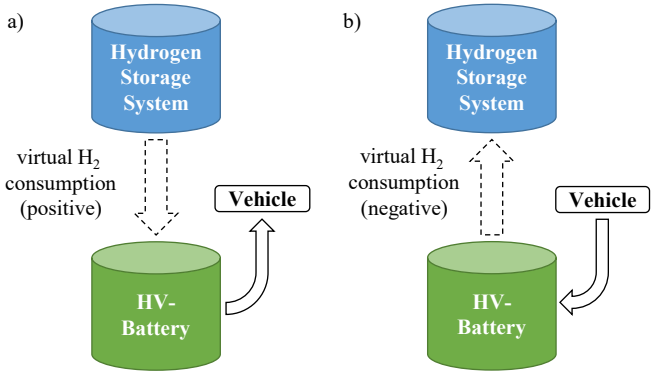

Figure 6 Principle of the ECMS a) discharging and b) charging of the HVB

The ECMS follows the approach that equivalence factors are used to establish equality between the actual hydrogen consumption of the FCS and the electrical energy provided by the HVB. Depending on whether the HVB is currently being charged or discharged, the electrical power represents a future virtual fuel consumption or a future virtual fuel saving. The equivalent fuel consumption at any given time t can be determined with equation 1:

$$\dot{m}_{f,equ}(t) = \dot{m}_{FCS}\left(P_{FCS}(t)\right) + \cdots + s_{dis}(t)\frac{1}{\eta_{HVB}(P_{HVB})}\frac{P_{HVB,pos}(t)}{Q_{lhv}} + \cdots + \frac{s_{chg}(t)\eta_{HVB}(P_{HVB})P_{HVB,neg}(t)}{Q_{lhv}} \quad (1)$$

where,

$\dot{m}_{f,equ}$ …	equivalent fuel consumption
$\dot{m}_{FCS}$ …	hydrogen consumption of the FCS
P_{FCS} …	output power of the FCS
P_{HVB} …	output power of the HVB
s_{dis} …	equivalence factor for the case of discharge
s_{chg} …	equivalence factor for the case of charge
η_{HVB} …	efficiency of the HVB
Q_{lhv} …	lower heating value of H_2 at 25 °C (119.95 MJ/kg)

For both EMSs presented, a parameter set exists that gives the best result regarding the objective of the EMS (e.g., minimization of

hydrogen consumption, reduction of the dynamic operation of the FCS) for the considered driving cycle. For the PFS, this parameter set is represented by parameters $P_{FCS,\,min}$, and SOC_{low}. In the ECMS, the best result can be found with an optimal pair of equivalence factors (s_{dis} and s_{chg}). The particle swarm optimization algorithm, implemented in MATLAB [50], is used to solve this optimization problem. This algorithm enables the determination of a global extremum (e.g., minimum hydrogen consumption) while considering specific constraints (e.g., power limits, charge-sustaining). In the optimization process, the parameters are varied until the best solution is reached. For the comparability of results, the charge-sustaining of the HVB is defined as the crucial constraint of the optimization problem. Here, the SoC of the HVB must reach the same value at the end of the drive cycle as at the beginning. Simulation results with a lower SoC are penalized and, thus, are not favorable for the optimization algorithm.

In the scope of the systematic development approach, the designed EMSs need to be evaluated. Therefore, the FCiL test methodology, which is presented later, is selected in this article. For this purpose, some rules must be added to the EMSs for practical reasons. A hysteresis with a minimum runtime of FCS for 3 seconds and a minimum shutdown period of 2 seconds is implemented to mitigate a permanent switching on and off of the FCS. If the EMS wants to shut down the FCS and the required runtime is not reached, the FCS solely provides the power demand. Furthermore, an automatic shutdown is intended for negative driver power demands.

Powertrain

The powertrain model can be further divided into the following sub-models the differential and transmission, E-Machine, the power electronics (inverter and DC/DC converters), the high-voltage battery, the fuel cell system, and the auxiliary consumers. In modeling, special care was taken to ensure that the full-vehicle model is suitable for pure simulative investigations and FCiL operation on the test stand. Further requirements for the design of the full-vehicle model were modularity, scalability, and real-time capability. Based on modularity, sub-models like the EMS can be easily exchanged and quickly integrated into the full-vehicle model through defined interfaces. The scalability of the powertrain components allows a comprehensive influence analysis of the different powertrain concepts regarding hydrogen economy. The real-time capability of the model must be ensured for FCiL operation on the test stand and requires a computationally efficient model.
Thus, all energy converters are modeled with quasistatic efficiency maps. The efficiency-based modeling approach generally enables computational-efficient simulations for fuel economy predictions of complex powertrain topologies. Moreover, this method provides accurate simulation results. Hence, it is widely used for developing powertrain concepts and EMSs for FCHEVs [51, 52]. Furthermore, due to the low numerical effort [36], it is also suitable for real-time applications such as Hardware-in-the-Loop simulation.

Transmission and Final Drive

The transmission and the final drive are combined into one sub-model with a total gear ratio of 8.779 [53], and an overall efficiency of 96 % is assumed.

E-Machine

The E-Machine is the core element of the electric propulsion system. A permanent magnet synchronous machine is modeled with generic data for the investigations. The EM is described using an efficiency map-based approach for an electric motor/generator. Figure 7 shows the efficiency map with the full-load characteristic curves for the motor and generator operation of the EM.

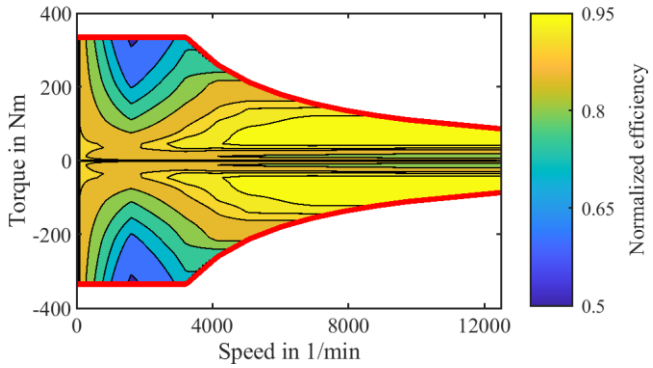

Figure 7 Efficiency map of the E-Machine

In the motor operation of the EM, the maximum torque is 335 Nm. The motor and generator operation of the EM is limited to a top speed of 12 500 1/min by the internal control of the EM. In both generator and motor operation of the EM, efficiencies greater than 90 % are achieved over a wide operating range.

Power Electronics

In the inverter model, only the power losses are considered. The inverter's efficiency typically has a maximum value of 99 % and remains above 90 % for most operating ranges [2]. Hence, a constant efficiency of 97 % is assumed over the entire operating range.
The HV DC/DC converters for the FCS and HVB are modeled with a constant efficiency of 97 %. In contrast, the efficiency of the LV DC/DC converter, which supplies the auxiliary consumers with power from the HV DC bus, is assumed to be 92 %.

High-Voltage Battery

The HVB or traction battery is modeled using a steady-state equivalent circuit consisting of an ideal voltage source and an internal resistor connected in series, as shown in Figure 8. The model of the HVB used in this article applies the quasi-static battery model at the cell level, allowing easy scalability for component sizing studies. Here, the energy content of the HVB is varied based on the number of cells and their configuration within the battery pack.

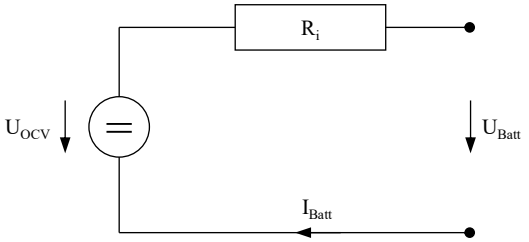

Figure 8 Equivalent circuit of the HV battery

The modeled battery is a nickel-metal-hydride battery in the default configuration with a nominal voltage of 224.8 V and a nominal energy content of 1.6 kWh. The battery pack is realized with 34 modules connected in series. Each module consists of a series

connection of 6 single cells with a nominal voltage of 1.2 V and a rated capacity of 6.5 Ah. The open circuit voltage and internal resistance are based on the data presented in [54]. Figure 9 shows the open circuit voltage (OCV) and the internal resistance for charging (R_{chg}) and discharging (R_{dis}) of a single cell. In addition, to consider the influence on the mass of the whole powertrain in the case of scaling the HVB, a gravimetric energy density of the battery pack of around 34 Wh/kg is assumed. This assumption is based on the data available in [55] for a NiMH battery pack with a nominal energy content of 1.6 kWh, which corresponds to the default configuration for the investigations in this study.

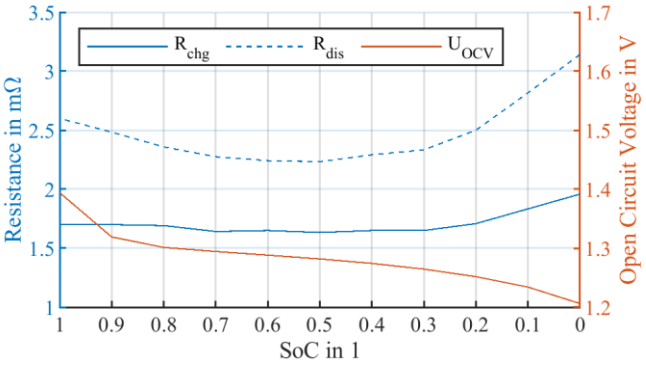

Figure 9 OCV and internal resistance of a battery cell according to the SoC

Fuel Cell System

A PEMFC system with a maximum output power of 110 kW is considered the basic variant for the study. The FCS mainly consists of an FC stack and three subsystems air supply, hydrogen supply, and thermal management. The modeled FCS is a scaled version of a commercial 22 kW FCS implemented on the test stand. This means that for the base variant of the investigated FCS, a scale factor of 5 (= 110 kW/22 kW) is in the FCiL platform applied. Further details regarding the FCS implemented on the test stand are outlined in the description of the FCiL platform later in this article. To model the FCS, a map-based approach is used. The model's input is the electrical power requested by the EMS, and the output is the hydrogen consumption. First, the required load current is determined as a function of the net output power of the FCS. This is done by using a look-up table indexed to the polarization curve, which characteristically describes the performance of the FCS. Figure 10 shows the polarization curve and the relationship between net output power and load current of the modeled FCS with a maximum power of 110 kW. As indicated before, the data presented in Figure 10 are scaled measurement data obtained with the FCS with 22 kW implemented on the test stand.

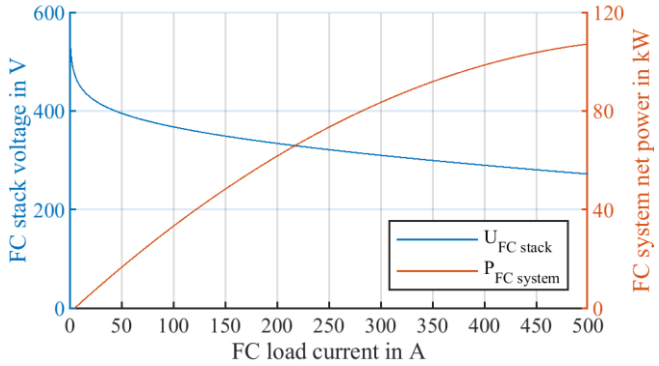

Figure 10 Polarization curve of the fuel cell stack

Once the load current is evaluated the hydrogen consumption of the FCS can be calculated using equation 2:

$$\dot{m}_{H2} = \frac{I_{FC} \cdot M_{H2}}{\upsilon \cdot F} \cdot n_{cell} \tag{2}$$

where,

$\dot{m}_{H2}$ … hydrogen consumption of the FCS in g/s

I_{FC} … load current of the FCS in A

M_{H2} … molar mass of hydrogen (2.02 g/mol)

υ … number of electrons transferred from each mole of hydrogen (2)

F … Faraday constant (96 485 C/mol)

n_{cell} … cell count of the FC system in 1

For the component sizing study, this model also considers the increase, respectively, the decrease in mass as it is scaled up or down. To this end, a value of 0.32 kW/kg is assumed for the gravimetric power density of the FCS. FCSs realized as stand-alone modules, typically have values of 0.28 to 0.59 kW/kg [56, 57, 58].

Auxiliary Consumers

While driving, some auxiliary consumers, such as lighting systems, power steering, and entertainment systems, require energy for their operation. In an FCHEV, this is provided in the form of electrical energy. To consider the auxiliary consumers, a constant power demand of 700 W is assumed and set up in the model as a continuous load drawn from the LV DC bus.

Vehicle Dynamics

Assuming that the vehicle is a point mass, the equilibrium of forces for the longitudinal motion can be described with the following equation 3:

$$m_{equiv,veh} \frac{dv_{veh}}{dt} = F_{trac} - F_{aero} - F_{roll} - F_{grade} \tag{3}$$

where,

$m_{equiv,veh}$ … equivalent mass of the vehicle in kg

$\frac{dv_{veh}}{dt}$ … acceleration of the vehicle in m/s²

F_{trac} … tractive force in N

F_{aero} … aerodynamic drag in N

F_{roll} … rolling resistance in N

F_{grade} … grade force due to road slope in N

By dividing with the equivalent mass of the vehicle and integrating equation 3 according to time, the current vehicle speed can be calculated with the knowledge of the resulting resistance force for each time step. The equivalent mass corresponds to the sum of the test and rotating mass of the vehicle. For the investigations, the parameters of the 2016 Toyota Mirai are taken from [35], and the equivalent test mass is calculated according to [59]. The resulting resistance force is modeled with a data-driven approach based on measurement data and can be described as a function of the vehicle velocity with the following equation 4:

$$F_{res,road} = F_0 + F_1 \cdot v_{veh} + F_2 \cdot {v_{veh}}^2 \quad (4)$$

where,

F_{res} … resulting road load force in N

v_{veh} … vehicle velocity in km/h

F_0 … road load coefficient in N

F_1 … road load coefficient in N/(km/h)

F_2 … road load coefficient in N/(km/h)²

The road load coefficients are evaluated using a coast-down test on a flat track within the study [35]. Table 1 lists all relevant data regarding vehicle dynamics.

Table 1 Key parameters of the full-vehicle model

Equivalent test mass	1904.5 kg
Road load coefficient F_0	169.17 N
Road load coefficient F_1	0.3491 N/(km/h)
Road load coefficient F_2	0.0319 N/(km/h)²
Dynamic wheel radius	0.33415 m

Fuel Cell-in-the-Loop Platform

In this study, the reduced-scale HiL approach is selected for the FCiL platform. Here, the physical hardware available on the test stand is an FCS with a maximum power lower by a scaling factor than the original FC system in the powertrain. With this FCiL test methodology, cost-effective investigations can be made at a very early stage of development compared to a platform with a full-scale FCS. In addition, as part of the powertrain design phase, the reduced-scale FCiL platform offers the possibility of investigating FCS with different output power rates instead of just one specific FCS. Overall, this approach allows a cost-efficient and diverse use in development.

Setup

Figure 11 shows the schematic layout of the FCiL platform. This mainly consists of two subsystems. The first subsystem represents the actual physical hardware available, the FCS. The FCS is implemented on a test stand consisting of a 30 kW PEMFC stack, a hydrogen supply system, an air-supply system, the cooling circuits, and the measurement and control system. The load point of the FC system is set by a dynamic DC/AC inverter (battery simulator). The battery simulator feds the electrical power generated by the FC system during operation into the electricity grid. An additional power supply system supplies the balance of plant components (e.g., air compressor, hydrogen recirculation pump, coolant pump) with electrical power. A more detailed description of the test stand can be found in [60, 61].

The second subsystem is the real-time simulation of the remaining FCHEV. This includes the remaining powertrain components of the FCHEV, the driver model, the driving cycle, the EMS, and a test stand controller. The latter is the interface between the simulation and the test stand. It sets the load point of the FC system. In addition, the following function is implemented in the test stand controller for application reasons. If the EMS triggers a shutdown of the FCS, then the FCS is put into standby mode. In this standby mode, the FCS is operated at a low load current of 20 A. It remains in this standby state until the next trigger for a switch-on comes from the EMS.

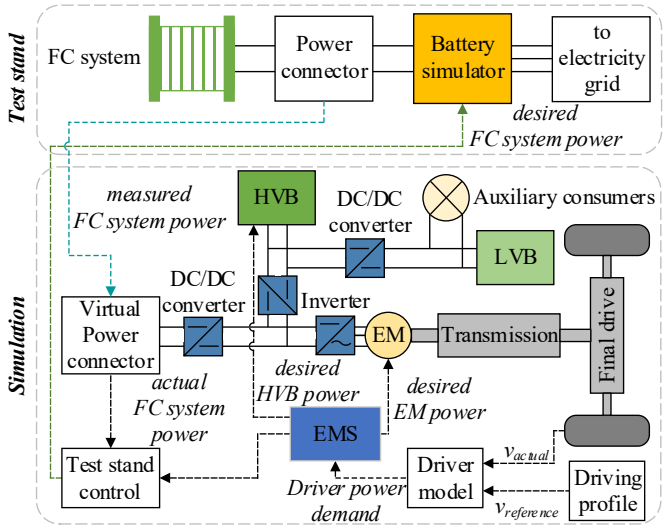

Figure 11 Principle layout of the FCiL platform

Functionality

In FCiL operation, the real-time capable simulation model, which runs on a real-time target computer, determines the electrical power demand of the FCS. The information about the power demand of the FCS is sent from the real-time target computer to the battery simulator. The battery simulator then sets the load point of the FCS. The measurement data from the sensors installed on the FCS test stand to determine the actual electrical power are transmitted to the simulation model via the interface of the real-time target computer. This data is further processed to react to the actual measured behavior in the simulation model, e.g., with a different load point. Thus, with the FCiL platform, the accurate operation of the FCS can be simulated in a vehicle environment, and the impacts, such as on

hydrogen consumption or dynamic behavior, can be evaluated experimentally.

Validation of the FCHEV Simulation

This section presents the evaluation of the vehicle dynamics model and part of the powertrain model from the final drive to the E-Machine to obtain valid simulation results. Additionally, the performance of the calibrated driver model is determined.

Validation of the Vehicle Dynamics and Part of the Powertrain

For the validation, measurements from a commercially available FCHEV on a chassis dynamometer in a standardized driving cycle (ADAC Eco-Test cycle) are taken from [35]. In Figure 12, the measured and simulated electrical power of the E-Machine for the ADAC Eco-Test driving cycle are compared. It can be seen that the simulation results agree well with the measurement results.

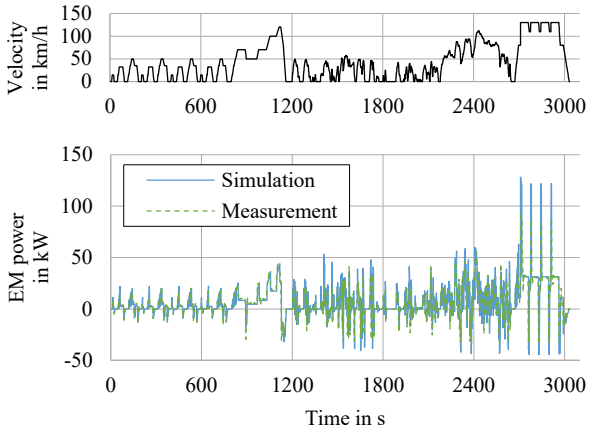

Figure 12 Validation of the FCHEV model in the ADAC Eco-Test cycle

Furthermore, the simulated and measured energy demand of the E-Machine for the entire drive cycle is compared. The comparison is listed in Table 2.

Table 2 Validation results of the FCHEV model in the ADAC Eco-Test cycle

Result	Measurement	Simulation	abs. Deviation
Distance traveled in km	35.5	35.6	0.3 %
Energy demand in kWh	5.97	5.92	0.8 %
Specific energy demand in kWh/100 km	16.82	16.63	1.1 %

It can be seen that there is a deviation of only 1.1 % between the simulation and the measurement result regarding the specific energy demand of the E-Machine. There are two main reasons for the discrepancy. One reason is that simplifying model assumptions are made, which inevitably leads to a difference between simulation and reality. The second reason is that, due to the limited information in the literature available, in modeling data sets are used that only approximately correspond to the data of the actual vehicle. Due to the minor deviation of 1.1 %, it can be concluded that the model represents the actual behavior of the existing powertrain. In summary, the validation results demonstrate the sufficient level of detail of the full-vehicle model.

Validation of the Driver Model

The controller parameters are calibrated to minimize the deviation between the reference and the actual vehicle velocity. The calibration and validation of the driver model are done through simulation in the WLTC. To determine the control quality, the maximum deviation of the velocity with a tolerance of +- 2 km/h, as required by [59], is the crucial criterion. The simulation result is presented in Figure 13. The evaluation shows a maximum absolute deviation between the reference and simulated velocity of 0.4 km/h. This is within the permissible tolerance mentioned before and confirms the proper calibration of the driver model.

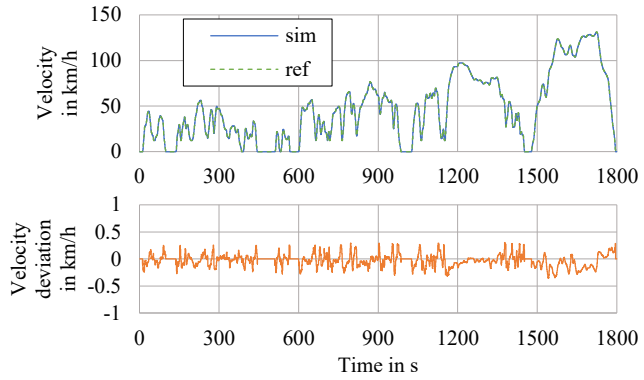

Figure 13 Validation of the driver model in the WLTC

Results and Discussion

In this section, selected EMSs and concepts of the powertrain are tested and evaluated in the WLTC by combining the experimental investigations with the FCiL operation on the test stand and a preliminary numerical study. The pure simulations, where the quasistatic model of the FCS is implemented, are used to find optimal parameter sets of the EMS for each investigated variant separately with the particle swarm optimization algorithm, as mentioned earlier. This is done to overcome the influence of wrongly chosen EMS parameters on the result. Furthermore, EMS parameters need to be calibrated in such a way as to guarantee the charge-sustaining operation of the HVB for a valid comparison of the results. For the tests with the FCiL platform, the optimal parameters are implemented in the EMS of the real-time simulation model. All investigations with the FCiL platform are conducted in a warmed-up state of the FCS. In particular, the conceptual design of the powertrain using the FCiL test methodology focused on the effect of FCS and HVB sizes on hydrogen consumption. The scope of the investigation of the EMSs is on their optimization, considering the hydrogen consumption and the dynamic operation of the FC system.

The reference configuration for all investigations in this article is the previously described configuration of the FCHEV, essentially consisting of an FCS with a maximum power of 110 kW and an HVB with a nominal energy content of 1.6 kWh. Additionally, in the reference configuration of the FCHEV, the power follower scheme as EMS is implemented, and the gradient of FCS load current is limited to a maximum of 75 A/s. Figure 14 shows the evaluation results with the FCiL platform of the FCHEV with standard configuration in the WLTC. At the top of Figure 14, the electrical power of the EM and

the FCS net power over time for the FCiL test in the WLTC are depicted. The power follower strategy uses the FCS to provide the drive power solely from a minimum power demand ($P_{FCS, min}$) of 11.4 kW to high load demands. Below that, the HVB provides the required propulsion power. Furthermore, the bottom of Figure 14 shows that a charge-sustaining operation of the traction battery is ensured.

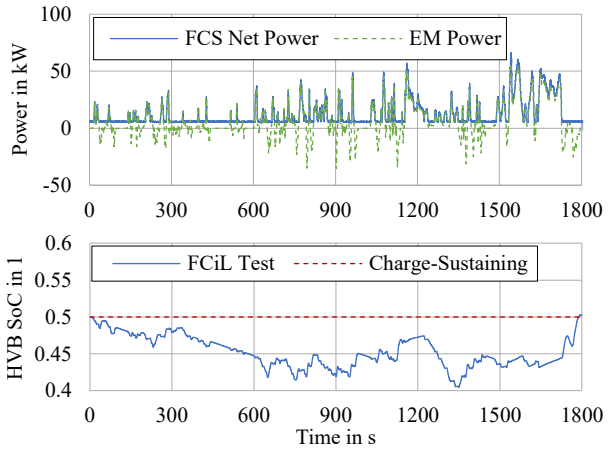

Figure 14 Results of the FCiL test with the FCHEV in the standard configuration in the WLTC

Sizing of Powertrain Components

A sensitivity analysis with the FCiL platform is conducted to obtain an optimal sizing of powertrain components. Starting from the reference configuration of the powertrain, only one parameter is varied for the investigated variant. This is done to determine the parameter's influence on hydrogen consumption precisely. In the sensitivity analysis, the FCS maximum power varies from 88 to 132 kW, and the HVB nominal energy content ranges from 0.8 to 2.4 kWh. In addition, two promising parameter combinations are investigated: the 132 kW FCS combined with the 0.8 kWh HVB and the 88 kW FCS combined with the 2.4 kWh HVB. It is assumed that the disadvantages of a reduced FCS maximum power or reduced HVB nominal energy content can be compensated by an increased HVB nominal energy content, respectively, increased FCS maximum power. The remaining combinations are not considered beneficial and thus are not investigated further. This is because they would severely limit the functionality (88 kW FCS combined with 0.8 kWh HVB), or the effort is likely to be disproportionate to the benefit in terms of hydrogen consumption (132 kW FCS combined with 2.4 kWh HVB). The powertrain sizing analysis also considers the effect on powertrain mass. In Table 3, the results of the study are depicted.

Table 3 Relative hydrogen consumption in % for component sizing in the WLTC

		FCS max. power		
		88 kW	*110 kW*	*132 kW*
HVB nominal energy content	*0.8 kWh*	-	102.1	102.4
	1.6 kWh	101.1	100	100
	2.4 kWh	100.9	100.1	-

A good result regarding a minimum hydrogen consumption by sizing the powertrain components in the WLTC is achieved with the FCS maximum power of 110 kW and the HVB nominal energy content of 1.6 kWh. The most significant negative impact on hydrogen consumption is for a configuration with an HVB with an energy content of 0.8 kWh and an FCS with a maximum power of 132 kW. This is mainly related to the limited performance capability of the HVB. Figure 15 shows a deceleration phase in the WLTC between 790-800 s, where the power limits of the different battery variants can be seen.

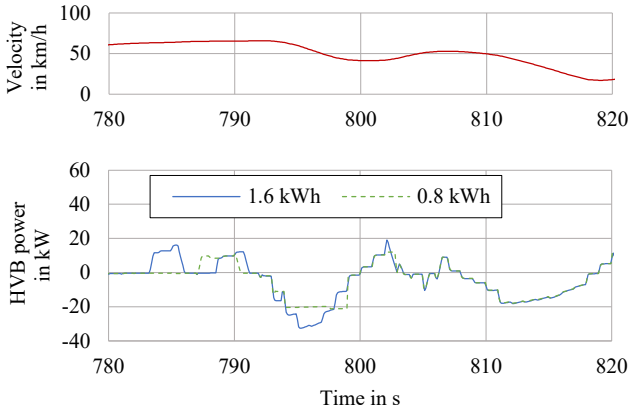

Figure 15 Comparison of different HVB sizes in the WLTC

Furthermore, an FCS with reduced maximum power leads to a significant increase in hydrogen consumption. This is because the load point of FCS with reduced maximum power must be set to a higher load current to achieve the same output power as in the reference configuration of the FCS. Therefore, the FCS with the reduced maximum power is operated at a lower efficiency, as shown in Figure 16.

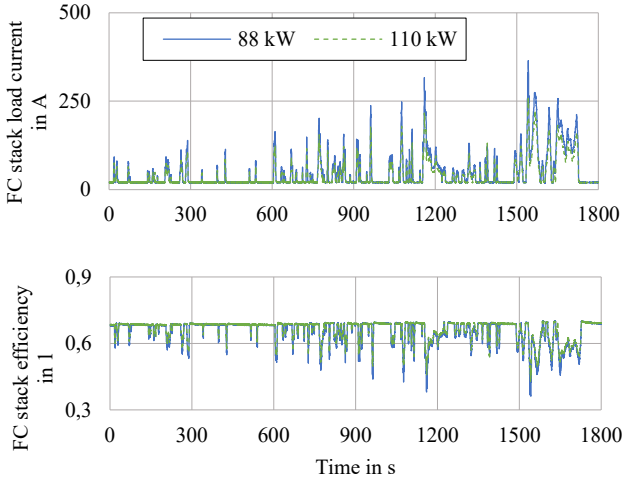

Figure 16 Comparison of different FCS sizes in the WLTC

Moreover, an increase in the FCS maximum power or the HVB nominal energy content does not influence hydrogen consumption significantly compared to the reference configuration. No significant gain could be achieved here since the WLTC is a driving cycle with low to medium load requirements. Therefore, the reference configuration of the FCS with 110 kW already operates under conditions of high efficiency, as shown in Figure 16. In addition, the reference configuration of HVB with 1.6 kWh is sufficient to meet its requirements as buffer energy storage (recuperation and support of the FCS) in the WLTC.

Optimization of the EMS

The trade-off behavior between minimum hydrogen consumption and reduced dynamics of the FC system is investigated to optimize the EMS. Hence, the FCS's maximum allowed load current gradient varies from 50 A/s to 100 A/s. In addition, two different EMSs are compared concerning hydrogen consumption in the WLTC. In Table 4, the results of the optimization of the EMS are depicted.

Table 4 Relative hydrogen consumption in % for optimization of the EMS in the WLTC

		FCS max. allowed current gradient		
		50 A/s	*75 A/s*	*100 A/s*
EMS	*PFS*	100.8	100	100
	ECMS	-	98.4	-

It is found that starting from the reference configuration of a maximum allowed load current gradient of the FCS of 75 A/s with a reduction by one-third, the additional consumption is only around 0.8 %. The limitation of the FCS load current gradient is realized with the hybrid function phlegmatization. Here, the HVB covers the driver's fast power demand, while the FCS follows the new power demand more slowly. Figure 17 shows two exemplary phases in the WLTC where a fast power demand for acceleration occurs. It can be seen that with an allowed FCS load current gradient of 50 A/s, the FC stack load current is raised more slowly compared to the variant with an allowed FCS load current gradient of 100 A/s. Hence, the HVB must supply more power to compensate for the difference between the power demand of the E-Machine and the FCS power output. As a result, the energy drawn from the battery to reduce the dynamic operation of the FCS is no longer available to minimize hydrogen consumption. In summary, reducing the dynamics of the FCS costs hydrogen. Nevertheless, it is found that a reasonable compromise can be achieved between reduced degradation of the FCS due to highly dynamic operation and only a small simultaneous increase in hydrogen consumption.

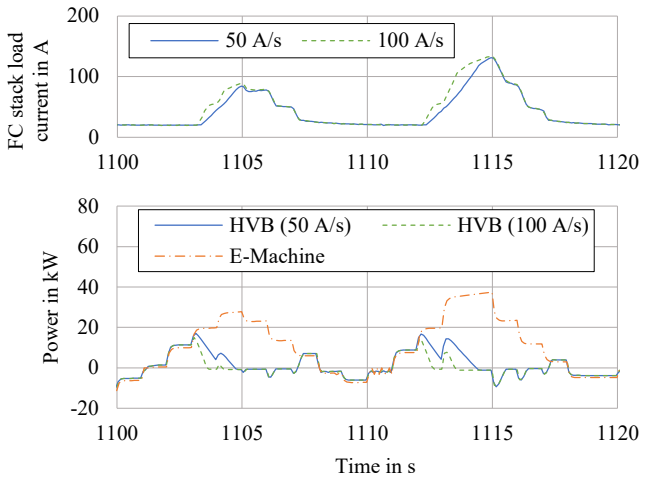

Figure 17 Comparison of different phlegmatization rates in the WLTC

Furthermore, it is shown that using the ECMS reduces hydrogen consumption by 1.6 % compared to the PFS for the same powertrain configuration. To achieve an optimal result with the ECMS regarding minimum hydrogen consumption, the optimal pair of equivalence factors of the ECMS is determined using the particle swarm optimization algorithm mentioned earlier. In this respect, the following values of the equivalence factors are found s_{chg} = 1.4018 and s_{dis} = 1.9806. A more detailed look at where the FCS is operated during the WLTC for both EMSs gives Figure 18. It can be seen that the ECMS tries to operate the FCS in the low to medium operating point range and, thus, in an efficient range when the power demand is low. Therefore, the ECMS carries out load point shifting of FCS at lower load requirements, thus charging the HVB. This means that sufficient energy in HVB is kept in advance, which can be used for load point shifting of FCS from higher to lower, more efficient loads when higher loads are required (e.g., highway driving).

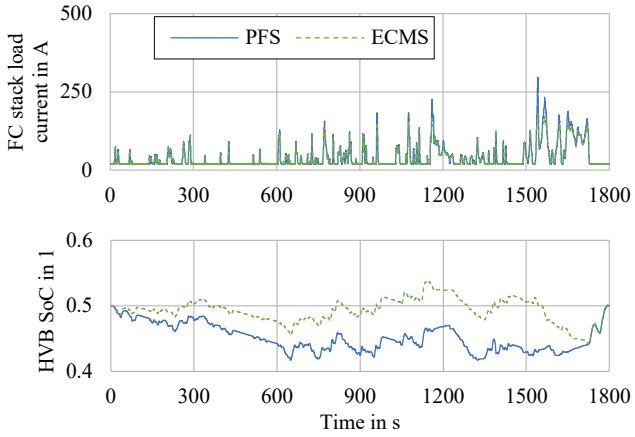

Figure 18 Comparison of the PFS and ECMS energy management strategy in the WLTC

Conclusions

This study presents a systematic development approach for the FCHEV powertrain and proves its feasibility as a tool for simultaneous numerical design and experimental evaluation under realistic operating conditions. To that end, a medium size FCHEV was modeled and validated. In parallel, a Fuel-Cell-in-the-Loop platform was designed and set up to evaluate the FCHEV powertrain concepts. In the first step, the FCiL test methodology was used to investigate the sizing of the FC system and the High-Voltage battery. It was found that for low-load driving cycles such as the WLTC, the combination of an FCS with a maximum power of 110 kW and an HVB with a nominal energy content of 1.6 kWh can achieve a good result in terms of minimum hydrogen consumption. This is mainly due to the following facts the FCS with 110 kW operates under high-efficiency conditions, and the HVB with 1.6 kWh is sufficient to meet its requirements as buffer energy storage (recuperation and support of the FCS) in the WLTC. Based on the virtual scaling of the powertrain components, the versatile applicability of the FCiL platform was demonstrated. Furthermore, a rule-based and an optimization-based energy management strategy were implemented and evaluated with the FCiL platform to study the impact of the EMS scheme on hydrogen consumption. It was shown that with the optimization-based EMS (equivalent consumption minimization strategy – ECMS), hydrogen consumption can be reduced by 1.6 % compared to the rule-based EMS (power follower strategy – PFS). The main reason is that the ECMS uses load point shifting of the FCS to operate the FCS in high-efficient operating ranges. Moreover, the trade-off behavior between the hydrogen consumption and the dynamic operation of FCS was investigated for further optimization of the EMS. Reducing the dynamic operation of the FCS by one-third results in an additional consumption of only about 0.8 %. This shows a reasonable compromise between reduced degradation of the FCS due to highly-transient operation and only a small simultaneous

increase in hydrogen consumption. In summary, it is demonstrated that the presented FCiL test methodology offers an approach for a systematic design and evaluation of an FCHEV powertrain under realistic operating conditions. It can therefore contribute to reduce time and costs in the development process.

References

1. Dicks, A., and Rand, D. A. J., "Fuel Cell Systems Explained," (Hoboken, Wiley, 2018), doi:10.1002/9781118706992.
2. Hayes, J., and Goodarzi, G., "Electric Powertrain: Energy Systems, Power Electronics and Drives for Hybrid, Electric and Fuel Cell Vehicles," (Hoboken, Wiley, 2018), doi:10.1002/9781119063681.
3. Pollet, B.G., Kocha, S.S. and Staffell, I., "Current Status of Automotive Fuel Cells for Sustainable Transport," *Current Opinion in Electrochemistry* 16: 90–95, 2019, doi:10.1016/j.coelec.2019.04.021.
4. Padgett, E., and Gregory K., "Automotive Fuel Cell Targets and Status," *DOE Hydrogen and Fuel Cells Program Record* 20005, 2020.
5. Jiao, K., Xuan, J., Du, Q., Bao, Z. et al., "Designing the Next Generation of Proton-Exchange Membrane Fuel Cells," *Nature* 595: 361–69, 2021, doi:10.1038/s41586-021-03482-7.
6. Pei, P., and Huicui C., "Main Factors Affecting the Lifetime of Proton Exchange Membrane Fuel Cells in Vehicle Applications: A Review," *Applied Energy* 125: 60–75, 2014, doi:10.1016/j.apenergy.2014.03.048.
7. Zhao, Jian, and Xianguo Li., "A Review of Polymer Electrolyte Membrane Fuel Cell Durability for Vehicular Applications: Degradation Modes and Experimental Techniques," *Energy Conversion and Management* 199: 112022, 2019, doi:10.1016/j.enconman.2019.112022.
8. Enz, S., Dao, T.A., Messerschmidt, M. and Scholta, J., "Investigation of Degradation Effects in Polymer Electrolyte Fuel Cells Under Automotive-Related Operating Conditions," *Journal of Power Sources* 274: 521–535, 2015, doi:10.1016/j.jpowsour.2014.10.127.
9. Lorenzo, C., Bouquain, D., Hibon, S. and Hissel, D., "Synthesis of Degradation Mechanisms and of Their Impacts on Degradation Rates on Proton-Exchange Membrane Fuel Cells and Lithium-Ion Nickel–manganese–cobalt Batteries in Hybrid Transport Applications," *Reliability Engineering & System Safety* 212: 107369, 2021, doi:10.1016/j.ress.2020.107369.
10. Badji, A., Abdeslam, D.O., Chabane, D. and Benamrouche, N., "Real-Time Implementation of Improved Power Frequency Approach Based Energy Management of Fuel Cell Electric Vehicle Considering Storage Limitations," *Energy* 249: 123743, 2022, doi:10.1016/j.energy.2022.123743.
11. Tanaka, Y., Shimizu, R., Nomasa, H. and Inoue, M., "Development of the Second-Generation Mirai – A Wholly New Type of Environmentally Friendly Vehicle," *Toyota Technical Review* 66: 7-11, 2021.
12. Hong, B. K., and Kim, S. H., "Recent Advances in Fuel Cell Electric Vehicle Technologies of Hyundai," *ECS Transactions* 86: 3, 2018, doi:10.1149/08613.0003ecst.
13. Sulaiman, N., Hannan, M.A., Mohamed, A., Ker, P.J. et al., "Optimization of Energy Management System for Fuel-Cell Hybrid Electric Vehicles: Issues and Recommendations," *Applied Energy* 228: 2061–2079, 2018, doi:10.1016/j.apenergy.2018.07.087.
14. M. Bajzek, J. Fritz, and H. Hick, "Systems Engineering Principles," in *Systems Engineering for Automotive Powertrain Development*, (Cham, Springer International Publishing, 2021), 149–194, doi:10.1007/978-3-319-99629-5_7.
15. Zhu, D., Pritchard, E. G. D., and Silverberg, L. M., "A New System Development Framework Driven by a Model-Based Testing Approach Bridged by Information Flow," *IEEE Systems Journal* 12(3):2917-2924, 2016, doi:10.1109/JSYST.2016.2631142.
16. Etzold, K., Kürten, C., Thul, A., Müller, L. et al., "Efficient Power Electronic Inverter Control Developed in an Automotive Hardware-in-the-Loop Setup," SAE Technical Paper 2019-01-0601, 2019, doi:10.4271/2019-01-0601.
17. Mihalič, F., Truntič, M. and Hren, A., "Hardware-in-the-Loop Simulations: A Historical Overview of Engineering Challenges," *Electronics* 11(15): 2462, 2022, doi:10.3390/electronics11152462.
18. Gao, H., Zhang, T., Song, K., Niu, W. et al., "Real-Time Testing Technology of Powertrain System in Proton Exchange Membrane Fuel Cell Electric Vehicles: A Review," SAE Technical Paper 2019-01-0371, 2019, doi:10.4271/2019-01-0371.
19. Fagcang, H., Stobart, R., Steffen, T., "A review of component-in-the-loop: Cyber-physical experiments for rapid system development and integration," *Advances in Mechanical Engineering* 14(8): 16878132221109969, 2022, doi:10.1177/16878132221109969.
20. Millitzer, J., Mayer, D., Henke, C., Jersch, T. et al., "Recent Developments in Hardware-in-the-Loop Testing," in *Model Validation and Uncertainty Quantification, Volume 3. Conference Proceedings of the Society for Experimental Mechanics Series* (Cham, Springer International Publishing, 2018), 65–73, doi:10.1007/978-3-319-74793-4_10.
21. Hansmann, J., Millitzer, J., Rieß, S. and Balzer, L., "Symbiose virtueller und experimenteller Methoden für effizienteres Testen und Entwickeln," presented at Experten-Forum Powertrain: Simulation und Test 2019, Germany, October 23-24, 2019, doi:10.1007/978-3-658-28707-8_4.
22. Schultze, M., Hähnel, C. and Horn, J., "Application of a Hardware-in-the-loop DC/DC converter and microgrid simulation to a PEMFC," presented at 2016 IEEE International Energy Conference (ENERGYCON), Belgium, 04-08 April, 2016, doi:10.1109/ENERGYCON.2016.7513995.
23. Moore, R.M., Hauer, K.H., Randolf, G. and Virji, M., "Fuel Cell Hardware-in-Loop," *Journal of Power Sources* 162(1): 302–308, 2006, doi:10.1016/j.jpowsour.2006.06.066.
24. Moore, R.M., Randolf, G., Virji, M.B. and Hauer, K.H., "Fuel Cell Hardware-in-Loop for PEM Fuel Cell Systems." *ECS Transactions* 5(1): 309–19, 2007, doi:10.1149/1.2729013.
25. Jia, C., Cui, J., Qiao, W. and Qu, L., "A Reduced-Scale Power Hardware-in-the-Loop Platform for Fuel Cell Electric Vehicles," presented at 2021 IEEE Transportation Electrification Conference & Expo (ITEC), USA, 21-25 June, 2021, doi:10.1109/ITEC51675.2021.9490118.
26. Bernard, J., Delprat, S., Guerra, T.M. and Büchi, F.N., "Fuel Efficient Power Management Strategy for Fuel Cell Hybrid Powertrains," *Control Engineering Practice* 18(4): 408-417, 2010, doi:10.1016/j.conengprac.2009.12.009.
27. Odeim, F., Roes, J., Wülbeck, L. and Heinzel, A., "Power management optimization of fuel cell/battery hybrid vehicles with experimental validation," *Journal of Power Sources* 252: 333-343, 2014, doi:10.1016/j.jpowsour.2013.12.012.
28. Odeim, F., Roes, J. and Heinzel, A., "Power management optimization of an experimental fuel cell/battery/supercapacitor hybrid system," *Energies* 8(7): 6302-6327, 2015, doi:10.3390/en8076302.

29. Goyal, G., “Model Based Automotive System Integration: Fuel Cell Vehicle Hardware-In-The-Loop,” Master's Thesis, Arizona State University, 2014.
30. Kandidayeni, M., Macias, A., Boulon, L. and Kelouwani, S., “Efficiency upgrade of hybrid fuel cell vehicles’ energy management strategies by online systemic management of fuel cell,” *IEEE Transactions on Industrial Electronics* 68(6): 4941-4953, 2020, doi:10.1109/TIE.2020.2992950.
31. Rudolf, T., Schürmann, T., Schwab, S. and Hohmann, S., “Toward holistic energy management strategies for fuel cell hybrid electric vehicles in heavy-duty applications,” *Proceedings of the IEEE* 109(6): 1094-1114, 2021, doi:10.1109/JPROC.2021.3055136.
32. Jiang, H., Xu, L., Li, J., Hu, Z. et al., “Energy management and component sizing for a fuel cell/battery/supercapacitor hybrid powertrain based on two-dimensional optimization algorithms,” *Energy* 177: 386-396, 2019, doi:10.1016/j.energy.2019.04.110.
33. Xun, Q., Murgovski, N. and Liu, Y., “Joint component sizing and energy management for fuel cell hybrid electric trucks,” *IEEE Transactions on Vehicular Technology* 71(5): 4863-4878, 2022, doi:10.1109/TTE.2022.3218341.
34. Xu, L., Mueller, C.D., Li, J., Ouyang, M. et al., “Multi-objective component sizing based on optimal energy management strategy of fuel cell electric vehicles,” *Applied energy* 157: 664-674, 2015, doi:10.1016/j.apenergy.2015.02.017.
35. Geringer, B., Tober, W. “Studie zur messtechnischen Analyse von Brennstoffzellenfahrzeugen Toyota Mirai,” Vienna, Austria: Austrian Society of Automotive Engineers, 2019.
36. Guzzella, L., and Sciarretta, A., “Vehicle propulsion systems. Introduction to modeling and optimization. 3. Ed,” (Berlin, Heidelberg, Springer, 2013), doi:10.1007/978-3-642-35913-2.
37. Alyakhni, A., Boulon, L., Vinassa, J.M. and Briat, O., “A comprehensive review on energy management strategies for electric vehicles considering degradation using aging models,” *IEEE Access* 9: 143922-143940, 2021, doi:10.1109/ACCESS.2021.3120563.
38. Ali, A.M. and Söffker, D., “Towards optimal power management of hybrid electric vehicles in real-time: A review on methods, challenges, and state-of-the-art solutions,” *Energies* 11(3): 476, 2018, doi:10.3390/en11030476.
39. Li, H., Ravey, A., N'Diaye, A. and Djerdir, A., “A review of energy management strategy for fuel cell hybrid electric vehicle,” presented at 2017 IEEE Vehicle Power and Propulsion Conference (VPPC), France, 11-14 December, 2017, doi:10.1109/VPPC.2017.8330970.
40. Zhang, P., Yan, F. and Du, C., “A comprehensive analysis of energy management strategies for hybrid electric vehicles based on bibliometrics,” *Renewable and Sustainable Energy Reviews* 48: 88-104, 2015, doi:10.1016/j.rser.2015.03.093.
41. Teng, T., Zhang, X., Dong, H. and Xue, Q., “A comprehensive review of energy management optimization strategies for fuel cell passenger vehicle,” *International Journal of Hydrogen Energy* 45(39): 20293-20303, 2020, doi:10.1016/j.ijhydene.2019.12.202.
42. Tran, D.D., Vafaeipour, M., El Baghdadi, M., Barrero, R. et al., “Thorough state-of-the-art analysis of electric and hybrid vehicle powertrains: Topologies and integrated energy management strategies,” *Renewable and Sustainable Energy Reviews* 119: 109596, 2020, doi:10.1016/j.rser.2019.109596.
43. Luciani, S. and Tonoli, A., “Control Strategy Assessment for Improving PEM Fuel Cell System Efficiency in Fuel Cell Hybrid Vehicles,” *Energies* 15(6): 2004, 2022, doi:10.3390/en15062004.
44. D. Wu and S. S. Williamson, “Performance Characterization and Comparison of Power Control Strategies for Fuel Cell Based Hybrid Electric Vehicles,” presented at 2007 IEEE Vehicle Power and Propulsion Conference, USA, 09-12 September, 2007, doi:10.1109/VPPC.2007.4544097.
45. Hollweck, B., Korb, T., Kolls, G., Neuner, T. et al., “Analyses of the holistic energy balance of different fuel cell powertrains under realistic boundary conditions and user behaviors,” *International Journal of Hydrogen Energy* 44(35): 19412-19425, 2019, doi:10.1016/j.ijhydene.2019.02.009.
46. Paganelli, G., Guezennec, Y., and Rizzoni, G., “Optimizing Control Strategy for Hybrid Fuel Cell Vehicle,” SAE Technical Paper 2002-01-0102, 2002, doi:10.4271/2002-01-0102.
47. Li, H., Ravey, A., N’Diaye, A. and Djerdir, A., “Online adaptive equivalent consumption minimization strategy for fuel cell hybrid electric vehicle considering power sources degradation,” *Energy Conversion and Management* 192: 133-149, 2019, doi:10.1016/j.enconman.2019.03.090.
48. Lin, X., Wang, Z., Zeng, S., Huang, W. et al., “Real-time optimization strategy by using sequence quadratic programming with multivariate nonlinear regression for a fuel cell electric vehicle,” *International Journal of Hydrogen Energy* 46(24): 13240-13251, 2021, doi:10.1016/j.ijhydene.2021.01.125.
49. Han, J., Park, Y. and Kum, D. “Optimal adaptation of equivalent factor of equivalent consumption minimization strategy for fuel cell hybrid electric vehicles under active state inequality constraints,” *Journal of Power Sources* 267: 491-502, 2014, doi:10.1016/j.jpowsour.2014.05.067.
50. The MathWorks, Inc., “Particle Swarm Optimization Algorithm,” https://de.mathworks.com/help/gads/particle-swarm-optimization-algorithm.html, accessed Oct. 2022.
51. Hu, X., Zou, C., Tang, X., Liu, T. et al. “Cost-optimal energy management of hybrid electric vehicles using fuel cell/battery health-aware predictive control,” *IEEE transactions on power electronics* 35(1): 382-392, 2019, doi:10.1109/TPEL.2019.2915675.
52. Jinquan, G., Hongwen, H., Jianwei, L. and Qingwu, L., “Real-time energy management of fuel cell hybrid electric buses: Fuel cell engines friendly intersection speed planning,” *Energy* 226: 120440, 2021, doi:10.1016/j.energy.2021.120440.
53. Toyota Motor Corporation, “NEW MIRAI PRESS INFORMATION 2020,” https://global.toyota/en/newsroom/toyota/33558148.html?_ga=2.218554905.126298, accessed Oct. 2022.
54. Gray, T., Motloch, C. and Francfort, J., “2007 Toyota Camry-7129 Hybrid Electric Vehicle Battery Test Results,” No. INL/EXT-09-16113. Idaho National Lab. (INL), Idaho Falls, ID (United States), 2010.
55. Toyota Motor Corporation, “CAMRY Hybrid 2012 Model 2nd Generation Emergency Response Guide,” https://www.nfpa.org/-/media/Files/Training/AFV/Emergency-Response-Guides/Toyota/Toyota-Camry-HEV-2012-2014-ERG.ashx, accessed Oct. 2022.
56. Yoshida, K., Takahashi, T., Imanishi, H., Paquet, T. et al., “Toyota’s Strategy for Fuel Cell Technology and the Progress in the Second Generation Mirai,” presented at 30th Aachen Colloquium Sustainable Mobility 2021, Germany, October 04-06, 2021.
57. Ballard Power Systems, Inc. “FCmove™-HD,” https://www.ballard.com/docs/default-source/spec-sheets/fcmovetm.pdf?sfvrsn=77ebc380_4, accessed Oct. 2022.
58. PowerCell Sweden AB. “PowerCellution Heavy Duty System 100,” https://www.datocms-assets.com/36080/1636359357-heavy-duty-system-100-v221.pdf, accessed Oct. 2022.
59. European Commission. “Commission Regulation (EU) 2017/1151 of 1 June 2017 supplementing Regulation (EC) No. 715/2007 of the European Parliament and of the Council on

type-approval of motor vehicles with respect to emissions from light passenger and commercial vehicles (Euro 5 and Euro 6) and on access to vehicle repair and maintenance information, amending Directive 2007/46/EC of the European Parliament and of the Council, Commission Regulation (EC) No. 692/2008 and Commission Regulation (EU) No. 1230/2012 and repealing ....” *Off. J. Eur. Union* 175 (2017): 1-643.
60. Du, Z.P., Steindl, C. and Jakubek, S. “Efficient Two-Step Parametrization of a Control-Oriented Zero-Dimensional Polymer Electrolyte Membrane Fuel Cell Model Based on Measured Stack Data,” *Processes* 9, no. 4: 713, 2021, doi:10.3390/pr9040713.
61. Höflinger, J., Hofmann, P., and Geringer, B., “Experimental PEM-Fuel Cell Range Extender System Operation and Parameter Influence Analysis,” SAE Technical Paper 2019-01-0378, 2019, doi:10.4271/2019-01-0378.

Contact Information

Christoph Steindl
Institute of Powertrains and Automotive Technology
TU Wien
Getreidemarkt 9, 1060 Vienna, Austria
+43-1-58801-31525
christoph.steindl@ifa.tuwien.ac.at

Acknowledgments

The research leading to these results has received funding from the Mobility of the Future program. Mobility of the Future is a research, technology, and innovation funding program of the Republic of Austria, Ministry of Climate Action. The Austrian Research Promotion Agency (FFG) has been authorized for program management (grant number 871503).

Definitions/Abbreviations

ADAC	Allgemeiner Deutscher Automobil-Club
Batt	Battery
BEV	Battery Electric Vehicle
Chg	Charge
Dis	Discharge
ECMS	Equivalent Consumption Minimization Strategy
EM	E-Machine
EMS	Energy Management Strategy
FCEV	Fuel Cell Electric Vehicle
FCHEV	Fuel Cell Hybrid Electric Vehicle
FCiL	Fuel-Cell-in-the-Loop
FCS	Fuel Cell System
HEV	Hybrid Electric Vehicle
HiL	Hardware-in-the-Loop
HSS	Hydrogen Storage System
HUT	Hardware Under Test
HV	High-Voltage
HVB	High-Voltage Battery
LV	Low-Voltage
LVB	Low-Voltage Battery
OCV	Open Circuit Voltage
PEMFC	Polymer Electrolyte Membrane Fuel Cell
PFS	Power Follower Strategy
SoC	State of Charge
WLTC	Worldwide harmonized Light vehicles Test Cycle